A TWO-DIMENSIONAL ITERATIVE PANEL METHOD AND BOUNDARY LAYER MODEL FOR BIO-INSPIRED MULTI-BODY WINGS

Christopher J. Blower*[a], Akash Dhruv[a] and Adam M. Wickenheiser[a]
[a]Department of Mechanical & Aerospace Engineering,
The George Washington University, Washington, District of Columbia, 20052, USA

ABSTRACT

The increased use of Unmanned Aerial Vehicles (UAVs) has created a continuous demand for improved flight capabilities and range of use. During the last decade, engineers have turned to bio-inspiration for new and innovative flow control methods for gust alleviation, maneuverability, and stability improvement using morphing aircraft wings. The bio-inspired wing design considered in this study mimics the flow manipulation techniques performed by birds to extend the operating envelope of UAVs through the installation of an array of feather-like panels across the airfoil's upper and lower surfaces while replacing the trailing edge flap. Each flap has the ability to deflect into both the airfoil and the inbound airflow using hinge points with a single degree-of-freedom, situated at 20%, 40%, 60% and 80% of the chord. The installation of the surface flaps offers configurations that enable advantageous maneuvers while alleviating gust disturbances. Due to the number of possible permutations available for the flap configurations, an iterative constant-strength doublet/source panel method has been developed with an integrated boundary layer model to calculate the pressure distribution and viscous drag over the wing's surface. As a result, the lift, drag and moment coefficients for each airfoil configuration can be calculated. The flight coefficients of this numerical method are validated using experimental data from a low speed suction wind tunnel operating at a Reynolds Number 300,000. This method enables the aerodynamic assessment of a morphing wing profile to be performed accurately and efficiently in comparison to Computational Fluid Dynamics methods and experiments as discussed herein.

Keywords: morphing, adaptive panel method, bio-inspired, gust alleviation, wake relaxation scheme

INTRODUCTION

Since the inception of the Wright Brother's wing warping Flyer, aircraft designs and flight capabilities have continuously advanced due to the demand induced by the end users for an extended operational flight envelope. Initially, basic control surfaces including the traditional ailerons, rudders and elevator were applied and have now become part of the standard aircraft archetype. In addition to ailerons, rudder and elevator control surfaces used for basic flight control, flaps, slats and slots are employed to enable improved lift-to-drag ratios and reduce flight speeds during the take-off and landing. However, it has only been since the early 1980s that new airflow manipulation techniques have been applied to enable increased controllability and maneuverability to achieve specialized flight objectives for unmanned aerial vehicles (UAVs). The inspiration of these flow control methods were observed from avian flight and their ability to continuously deform their wing geometry depending on a series of localized variables, i.e. angle of attack, flight speed and desired trajectory. These techniques have been subsequently identified and developed by numerous research teams to enable wing morphing through active control of the wing's camber line geometry [1], thickness [2], sweep [3], span [4] and twist [5] to achieve the necessary aerodynamic coefficients for a complex maneuver or specific flight leg. However, for over a century, atmospheric turbulence and gusting flows have plagued manmade flight and remain the primary causes of UAV loss when operating at low altitudes and/or in cluttered environments [6].

Recently, additional attention has to been given to the assessment of morphing wing dynamics of avian flight and the study of bio-mimicry for advanced locomotion and maneuvering techniques for implementation on UAVs. Avian flow control consists of both the flapping motion that achieves propulsion and maneuvering and the contraction and relaxation of the muscles controlling the feathers orientation for manipulating the local air flow for gust alleviation and maneuvers [7–10]. From previous studies [10–13], the presence of flight feathers over the wing surface have been observed to aid a bird's ability to sense and influence the flow over its wings, thereby offering an effective method for localized flow control. Subsequently, a new bio-inspired gust alleviation and maneuverability system (GAMES) has been developed in which an array of feather-like flaps has been installed across the airfoil's upper and lower surfaces to mimic a bird's wing morphing abilities and enable delayed flow separation, enhanced

Bioinspiration, Biomimetics, and Bioreplication 2014, edited by Akhlesh Lakhtakia, Raúl J. Martín-Palma,
Proc. of SPIE Vol. 9055, 90550V · © 2014 SPIE · CCC code: 0277-786X/14/$18 · doi: 10.1117/12.2046564

flow control and maneuverability during UAV flight. Due to the number of moving lifting surfaces integrated into the wing design, an adaptive aerodynamic solver must be employed that can perform efficiently and accurately to calculate the aerodynamic coefficients of the wing while operating in the wide array of configurations available to the morphing aircraft. Currently, there are an array of solvers available for designing airfoils and assessing the flow around the wing profile [14], including finite element Navier-stokes flow solvers [15–18], conformal mapping [19–21], and panel methods [22–25]. While Navier-Stokes flow solvers enable the effects of viscosity to be taken into consideration around complex geometries, the complex mesh geometries required cause the simulations to be expensive, both financially and in time [26,27]. However, the implementation of potential flow panel methods has become a popular tool for modeling flow in the aerodynamic community. These numerical methods allow the flow characteristics over the body surface to be solved instead of the entire volume encapsulating the airfoil geometry, c.f. finite difference methods [20], thereby reducing computational time while maintaining accuracy.

This paper discusses the development of a two-dimensional iterative panel method with an integrated boundary layer model to assess the aerodynamic coefficients of a bio-inspired, two-dimensional feathered wing under various flight conditions. The goal of this adaptive aerodynamic solver is to be a robust tool to calculate the aerodynamic coefficients for complex morphing multi-element geometries and is validated by comparison to a conventional airfoil using existing panel method codes and wind tunnel measurements.

BIOINSPIRED MULTI-ELEMENT AIRFOIL OVERVIEW

The GAMES employs eight equally sized flaps distributed along the upper and lower surfaces of a NACA 4412 airfoil, thereby replacing the airfoil surface, standard flaps and ailerons. Each flap is designed to individually rotate about its respective hinge point, located at 20%, 40%, 60% or 80% of the chord length, into both the inbound airflow and the airfoil profile to enable a range of beneficial geometries that are unobtainable by a traditional airfoil. Due to the removal of the trailing edge flaps and ailerons, the GAMES performs the role of flight control and localized flow manipulation for gust alleviation simultaneously. The airfoil geometry for the GAMES has been developed in a three stage process using a single trailing edge (STE), a dual trailing edge (DTE) and multi-flap profile (MFP) geometry, as seen in Figure. 1a-c. This multi-stage evolution of the airfoil allows the aerodynamic characteristics to be assessed incrementally as the wing geometry increases in complexity between each stage. To ensure the GAMES's aerodynamic model is both accurate and robust, validation is performed against existing panel method codes, historical data and experimental wind tunnel results. For a detailed insight into the development of the DTE please refer to Blower and Wickenheiser [28–30].

The installation of the MFP enables the wing to perform new capabilities including aero-braking through the rotation of each flap into the inbound flow (Fig. 1d), drag minimization during gusting flow interaction at high angles of attack (Fig. 1e) and a wide array of asymmetric geometries (i.e. Fig 1f) to manipulate the airflow, thereby extending the operating envelope of lift, drag and pitching moment coefficients.

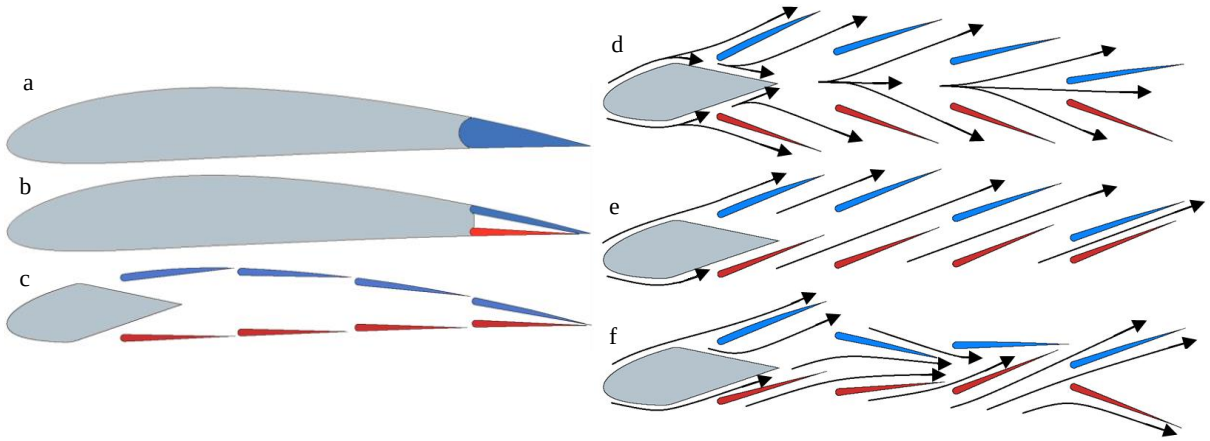

Figure 1: NACA 4412 with standard singular trailing edge flap (a) and the dual trailing edge flap configuration (b) and the eight-feathered multi-flap profile configuration (c). The GAMES airfoil with airflow path lines for an aero-braking geometry (d), minimal drag during flight at large angles of attack (e) and an asymmetric geometry (f).

MULTI-ELEMENT PANEL METHOD FOR SURFACE LOAD CALCULATION

For each flap configuration, the adaptive panel method (APM) incorporates the free-stream velocity, V_∞, angle of attack, α, and flap deflection angle, δ_x, where $x = 1,\ldots,8$, shown in Fig. 2. The Dirichlet boundary condition, which states the internal potential of each element must remain constant, is assessed at the collocation point located on each panel. Each element is discretized into panels using a cosine distribution applied to the panel's collocation points across both the upper and lower surfaces, defined from the leading to trailing edge of each element. During initial simulations, the panel method's sensitivity to the number of panels used in the discretization was assessed. In this assessment, a baseline model of a standard NACA 4412 airfoil was discretized using 5 to 1000 chord-wise panels per surface and the coefficient of lift was calculated to identify a panel number that offered a reduced computational time while ensuring the model remained accurate while operating over the desired range of angle of attack and free-stream velocity. The simulation results indicated that a panel count of 101 chord-wise collocation points distributed over each surface attained a coefficient of lift within 0.5% of the baseline model, Fig. 2a. Consequently, 101 panels are applied to each element of the MFP resulting in the panel length varying between $3.4\text{x}10^{-3}$ and $2.7\text{x}10^{-4}$, where the chord length has been normalized to 1, Fig. 2b. An increased panel density is applied to regions of high sensitivity, i.e. the leading and trailing edge, thereby ensuring an accurate velocity and pressure distribution are achieved. The APM implements a constant-potential doublet and source method with the Dirichlet boundary condition applied [20].

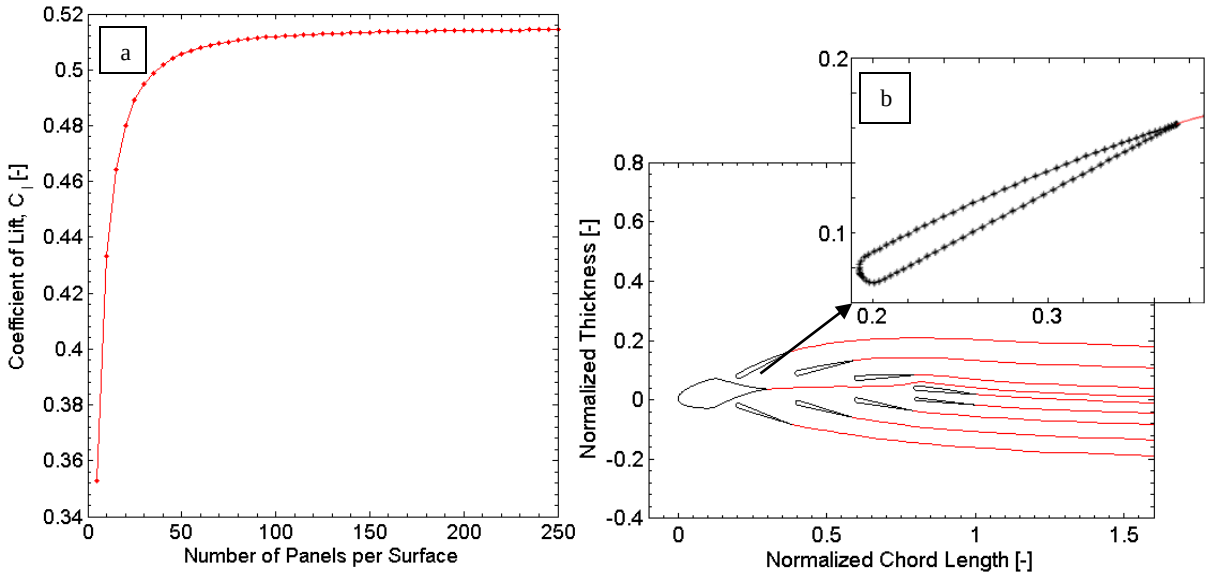

Figure 2: An assessment of the sensitivity and accuracy achieved for an airfoil's coefficient of lift with varying panel density(a) and the cosine distribution employed across each surface in a multi-element profile where α = 0°, δ_1=20°, δ_1=20°, δ_2=15°, δ_3=10°, δ_4=5°, δ_5=-20°, δ_6=-15°, δ_7=-10°, δ_8=-5°, for Re = 1E6 (b)

To calculate the coefficient of pressure across each element, the strength of the doublets and sources distributed across the airfoil's surfaces must initially be determined. The source strength is derived from the normal component of the free-stream flow at each panel's collocation point ($\sigma_j = \mathbf{n}_j \cdot \mathbf{Q}_\infty$). The panel's doublet strength is calculated by applying the impenetrability boundary condition at each collocation point [20].

$$\sum_{j=1}^{N} B_{ij}\sigma_j + \sum_{j=1}^{N} C_{ij}\mu_j + \sum_{k=1}^{N_w} B_{ik}\sigma_k + \sum_{k=1}^{N_w} C_{ik}\mu_k = 0 \qquad \text{(X)}$$

where B and C are the tangential-influence coefficients for each of the singularities on the airfoil elements and within the wake profile and the doublet strength, μ, and source strength, σ, are assessed relative to the panel location.

To enable the viscous boundary layer to be computed over the surface of the airfoil, the tangential velocity, u_i, is required to determine the boundary layer thickness and the resultant induced drag. The tangential surface velocity is calculated at each collocation point on both the airfoil and the wake through the summation of the velocity induced by each singularity and the tangential component of the free-stream velocity relative to the panel, $Q_{t\infty}$:

$$u_i = \frac{\mu_j - \mu_{j+1}}{\Delta l_j} + Q_{t\infty} \tag{X}$$

where Δl_j is the distance between neighboring doublet singularities.

WAKE RELAXATION SCHEME

Panel methods have been demonstrated to be sensitive to the panel distribution and the airfoil geometry [31–33]. Consequently, the panel distributions employed on the airfoil and along the wake are crucial to model the surface pressure and tangential velocity around an airfoil geometry is crucial to the calculation of the aerodynamic coefficients of lift, drag and moment.

For the development of an accurate aerodynamic solver, the complex interaction between the airfoil and the trailing wake must be assessed. As the free-stream flow interacts with both components, the aft wake induces an influence on the airfoil body and consequently effects both circulation strength required to keep the rear stagnation point at the airfoil's trailing edge, also known as the Kutta condition, and the pressure distribution over the airfoil's surface [20]. In traditional single-pass panel methods, a fixed von Kármán wake panel of infinite length (~1000c) is attached to the airfoil's trailing edge and aligned with either the trailing edge bisector angle or the free-stream velocity. The orientation of the wake is user defined and is dependent on the region of interest for the model; for example, a wake aligned with the airfoil's trailing edge bisector angle follows the trajectory of the fluid flow as it separates from the wing's upper and lower surfaces, thus accurately representing the near field wake velocity profile. However, as the velocity profile for the wake geometry is assessed further downstream, the airflow becomes dominated by the free-stream velocity, hence reducing the accuracy of the wake's downstream influence and violating the conservation of momentum principle, resulting in the overestimation of lift and underestimation of induced drag [34]. For the latter scenario in which the von Kármán wake panel is aligned with the free-stream flow immediately aft of the trailing edge, the opposite result is obtained in which the accuracy of the wake's influence improves the further downstream the wake is assessed [34].

To ensure that an accurate representation of the wake influence is achieved, the wake panels are aligned with the local velocity field, thereby satisfying the flow conditions both within the near- and far-field flows as well as satisfying the conservation of momentum principle [34,35]. The wake profile is discretized into 50 panels with a half-cosine distribution for 20c; beyond this length the turbulent wake is assumed to have dispersed, and, therefore, the flow is dominated by the free-stream velocity [20]. To maintain continuity in the panel density and convergence of the panel method, the first wake panel and the last airfoil panel are set to be the same length. A modified von Kármán wake panel (~980c) is applied to the end of the discretized wake and aligned with the free-stream flow. The installation of this wake panel maintains the desired infinite wake length, while preventing wake roll up from occurring near the airfoil body.

To date, there are two methods commonly employed to derive wake profiles behind an airfoil, the time-stepping scheme [36–38] and the spatial wake relaxation method [34,39,40]. The time-stepping wake relaxation scheme is typically applied to simulations assessing unsteady flows [37] or moving components, such as rotor blades or flapping wings, in which the wake profile is deforming with respect to time. For aerodynamic modeling of steady flow, an iterative spatial wake relaxation scheme is employed so that the initial discretized wake profile extends from the airfoil at the trailing edge bisector angle. During each iteration the local velocity vector field is derived from the normal and tangential velocities:

$$u = \frac{\mu}{2\pi}\left[\frac{z_i}{\left(x_i - x_j\right)^2 + z_i^2} - \frac{z_i}{\left(x_i - x_{j+1}\right)^2 + z_i^2}\right] - \frac{\sigma}{4\pi}\left[\frac{\left(x_i - x_j\right)^2 + z_i^2}{\left(x_i - x_{j+1}\right)^2 + z_i^2}\right] \tag{1}$$

$$w = \frac{-\mu}{2\pi}\left[\frac{x_i - x_j}{(x_i - x_j)^2 + z_i^2} - \frac{x_i - x_{j+1}}{(x_i - x_{j+1})^2 + z_i^2}\right] - \frac{\sigma}{2\pi}\left[\tan^{-1}\left(\frac{z_i}{x_i - x_{j+1}}\right) - \tan^{-1}\left(\frac{z_i}{x_i - x_j}\right)\right] \quad (2)$$

where the tangential and normal velocities, *u* and *w*, are calculated with relation to the x- and z- components of the panel collocation and end points, denoted by subscripts *i* and *j*, respectively. The panel velocity components are converted to the global coordinate system and added to the free-stream velocity (U_x and U_z), yielding the local velocity field in the wake. Each wake panel is subsequently rotated to align with the local velocity field and a new wake geometry is derived through the magnitude of the vertical and horizontal velocities:

$$x_j = x_{j-1} + (z_j - z_{j-1})\frac{u\sin\delta_p + w\cos\delta_p + U_z}{u\cos\delta_p + w\cos\delta_p + U_x} \quad (3)$$

$$z_j = z_{j-1} + (x_j - x_{j-1})\frac{u\sin\delta_p + w\cos\delta_p + U_z}{u\cos\delta_p + w\cos\delta_p + U_x} \quad (4)$$

This procedure is repeated until a convergence criterion is satisfied [35]; for the APM to achieve convergence, the final wake panel displacement must be less than 0.001 in the z-direction between sequential iterations. Any z-displacement smaller than this is considered to induce negligible effects on the airfoil's pressure distribution. For the baseline NACA 4412 airfoil the spatial relaxation scheme requires three iterations to converge, as shown in Fig 3.

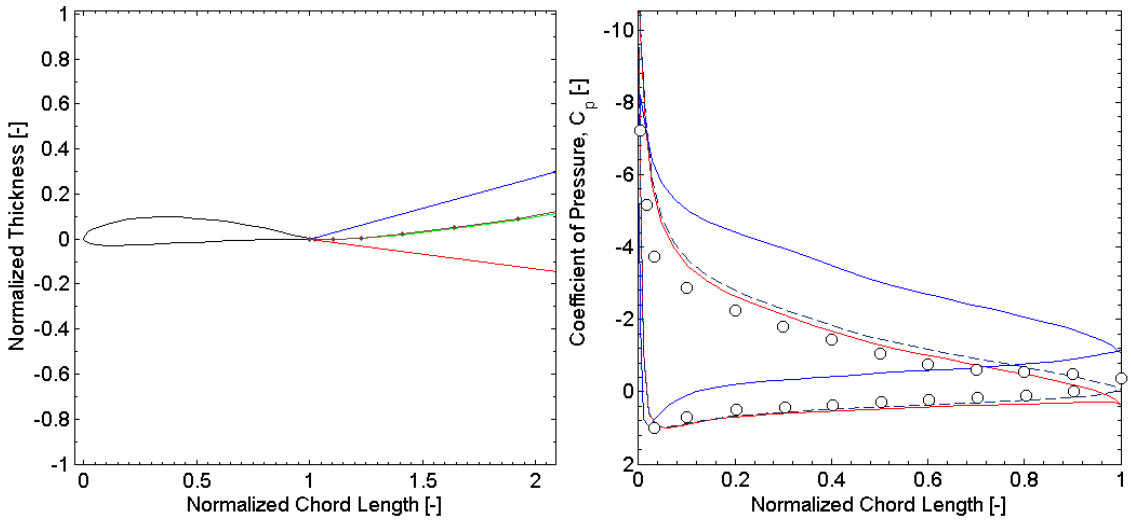

Figure 3: An iterative spatial relaxation scheme for a NACA 4412 airfoil at an angle of attack of 13.87° with an initial wake geometry aligned with the trailing edge bisector angle (red), the 2nd iteration (green) and the converged 3rd iteration (black-dotted). The free-stream wake profile (blue) is presented to demonstrate the upper bounds between which the wake profile will converge (a). The coefficient of pressure distribution of the spatial relaxation scheme (---) is compared to panel method profiles employing a wake aligned with the free-stream velocity (red) or the trailing edge bisector (blue), and experimental results (o)

The implementation of a spatial wake relaxation scheme has been demonstrated to supersede the accuracy of the single panel wake geometry and, consequently, achieve the closest results to experimental data for both coefficient of pressure and lift [41]. Validation of the relaxation scheme was performed for subsonic incompressible flows, ranging Re = 0.1-9.2E6, by the assessment of the coefficient of pressure distribution for a NACA 4412 against experimental data from wind tunnel testing [42,43], shown in Fig 3. The single wake panel methods that are aligned with the free-stream or trailing edge bisector angle demonstrated an average error across the airfoil surface, relative to the experimental results of 30% and 5.6% respectively, while the relaxation scheme achieved an average error of 5.2%. However, within the trailing 20% of the airfoil, where the highest panel sensitivity is incurred, this method achieves an error less than 4.0% versus the free-stream and bisector wake models that incurred 10.7% and 9.7% error, respectively.

The implementation of the wake relaxation scheme is extended to the MFP, thereby allowing the influence from each element and wake to be applied to the airfoil bodies and flow downstream. Each element has an arbitrary wake profile attached to the trailing edge that iteratively deforms to follow the streamlines around the complex downstream geometries. For a multi-element wake profile, the wake geometries are solved simultaneously, and the doublet/source influence is modified accordingly during each iteration. This technique enables the coefficient of pressure to be modeled accurately within a complex flow for a multi-element airfoil while operating in any configuration, shown in Fig. 4.

The MFP can be seen to mimic the external surface pressure of a basic NACA 4412 across each flap while in the rest configuration. Pressure spikes near the leading edge of each flap are a result of the accelerated flow passing between neighboring flaps, creating a slot flow. In addition, the internal surfaces can be seen to have a coefficient of pressure equal to one, meaning that the internal fluid flow is stagnant. For a MFP geometry in which all flaps are deflected into the inbound flow, pressure spikes are incurred at the leading edge of each flap; however, the internal surfaces are no longer stagnant as the inbound flow now has the capability to pass through the inside of the wing, indicated in Fig 4.

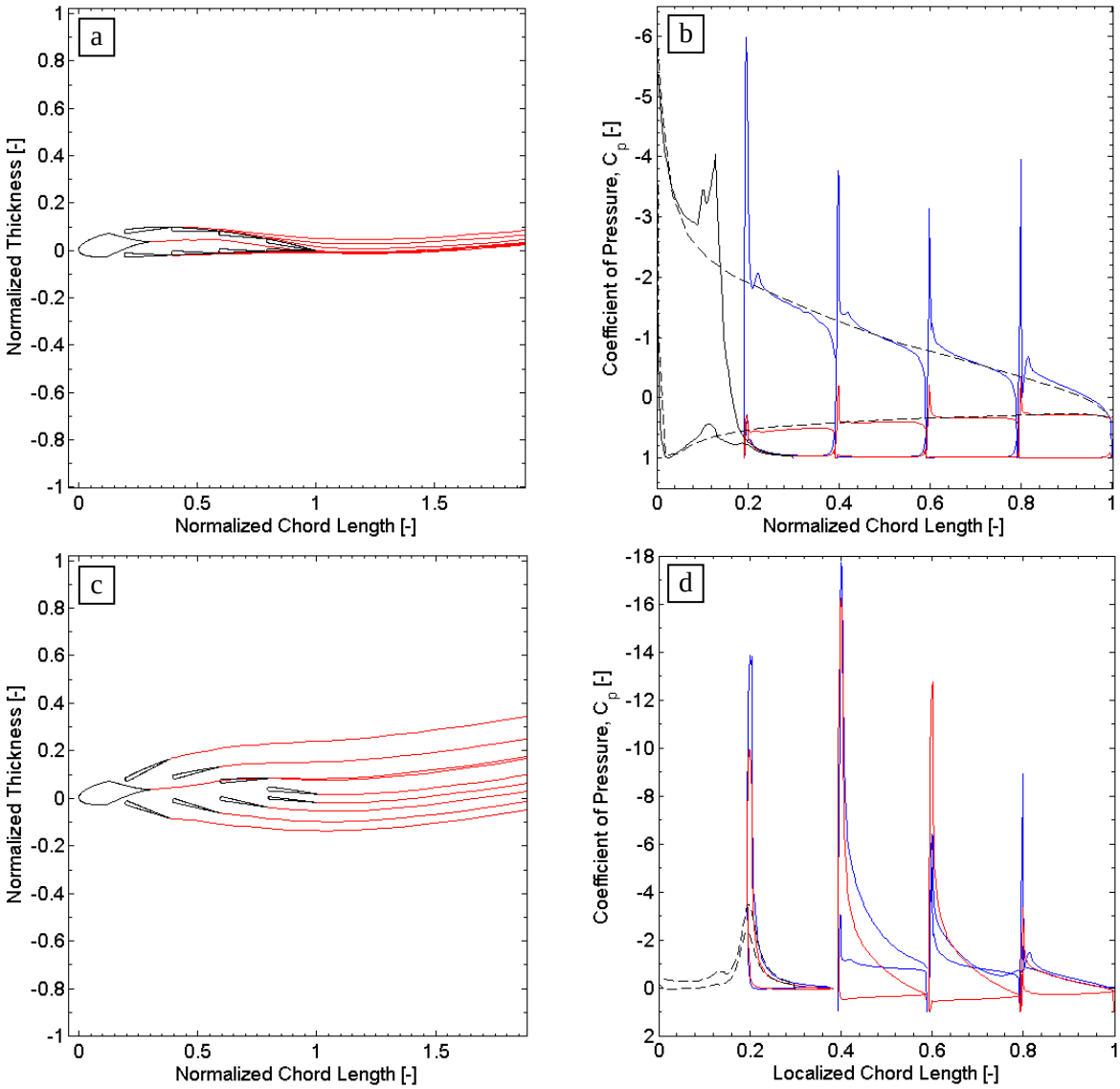

Figure 4: Wake relaxation scheme applied to the two-dimensional MFP using a constant-potential doublet/source panel method at rest configuration (a) and the resultant coefficient of pressure distribution compared to a traditional NACA 4412 (---) (b) and a MFP with flaps deflected to $\delta_1 = 20°$, $\delta_2 = 15°$, $\delta_3 = 10°$, $\delta_4 = 5°$, $\delta_5 = -20°$, $\delta_6 = -15°$, $\delta_7 = -10°$, $\delta_8 = -5°$ (c) and the coefficient of pressure distribution (d)

During certain configurations, a basic spatial wake relaxation scheme for a multi-element airfoil has been demonstrated to fail when the downstream separation distance between subsequent elements is less than 0.005c. This is due to the wake profile having an insufficient distance to allow the flow to bend around the downstream flaps, causing the wake to pass through the airfoil body and resulting in a violation of the impermeability boundary condition, depicted in Fig. 5a. To overcome this issue, after the first iteration of the spatial wake relaxation scheme has been completed, each wake is assessed for any interaction with neighboring flaps. In the cases where the wake collides with a flap, the point of interaction on the body's surface is defined as a stagnation point, as the wake is driven to divide and pass around the upper and lower surfaces. During subsequent iterations, the APM determines that no fluid flow can pass between the elements and therefore redistributes the surface panels from Fig.5b to encapsulate both the elements and the joining wake, while the aft wake maintained, shown in Fig. 5c. The relaxation scheme is repeated until convergence is achieved, after which the merged profile is divided, shown in Fig. 5d, and the coefficient of pressure for each element is calculated. This technique can be employed when complex geometries are selected where multiple wake-element interactions occur.

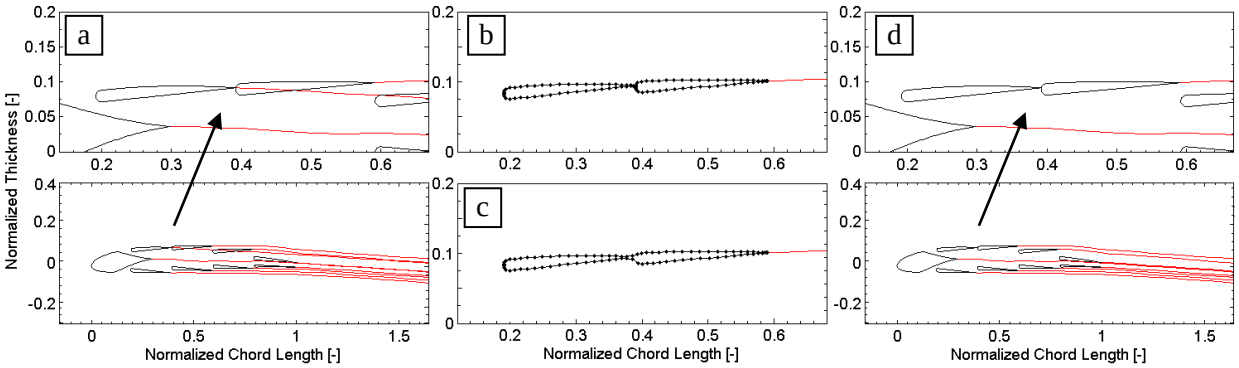

Figure 5: The APM modifies the wake-element geometry when interactions are incurred (a) by identifying the elements involved (b) and redistributing their panels to create a single body (c). When the wake relaxation scheme is complete the elements are separated and the single wake defined (d).

BOUNDARY LAYER THEORY

To model the viscous drag components induced over the MFP wing's surfaces accurately, a boundary layer model is employed. This method employs the coefficients of pressure and tangential velocity derived from the converged panel method to calculate boundary thickness and viscous drag.

Initially, each element is divided into an upper and lower surface that initiate at the element's stagnation point; this location is dependent on the free-stream velocity, the airfoil's angle of attack and flap configuration. Flow stagnation on each element is achieved when either the tangential velocity is equal to zero or a wake from an upstream body interacts with the surface of the element being assessed. Due to the number of possible flap configurations, and the potential boundary layer separation from an upstream element reattaching to elements downstream, the boundary layer is modeled forward to aft of the airfoil. The boundary layer growth is modeled with respect the arc length coordinate, *s*, which originates at the element's stagnation point.

To calculate the skin-friction drag, C_d, the dimensionless wall shear stress, also known as the coefficient of friction, c_f, is calculated across each element's surface. However, to calculate this parameter, the laminar, transition and turbulent regions must first be identified and modeled. The fluid flow is assumed to be laminar aft of the stagnation point; consequently Thwaites method is employed to model the growth of the momentum thickness, θ, and the dimensionless pressure gradient, λ, within this regime until either flow transition or separation occurs [44].

The boundary layer is predicted to separate when $\lambda(s) \leq -0.09$ [45], or to become turbulent when Michel's transition criterion is fulfilled for an incompressible flow with no heat transfer [44,46], given by

$$\mathrm{Re}_\theta > 1.174\left(1+\frac{22400}{\mathrm{Re}_s}\right)\mathrm{Re}_s^{0.46} \tag{5}$$

where Re_s is the arc length-dependent Reynolds Number and Re_θ is the momentum thickness-dependent Reynolds Number. These terms are defined as $\mathrm{Re}_s = \rho u s/\mu$ and $\mathrm{Re}_\theta = \rho u \theta/\mu$, respectively, where ρ is air density μ is kinematic viscosity and u is the tangential velocity derived from the APM.

Due to the flow complexities that exist within the transition region, the flow beyond the transition point is assumed turbulent [44] and modeled using Head's entrainment velocity method. The flow is assumed to remain turbulent until either the flow separates, when $H(s_s) \geq 2.40$ [44], reaches the trailing edge of the airfoil or incurs relaminarization due to adverse pressure [47–49]. Head's turbulent method requires the von Kármán momentum integral equation, Eq. 6, Ludwieg-Tillman's skin friction law, Eq. 7, Cebeci and Bradshaw's empirical shape factor and turbulent shape factor relationships, Eq. 8-10, are to be solved simultaneously to identify the boundary layer's momentum thickness, shape factor, *H*, turbulent shape factor, H_1, and coefficient of friction, c_f. These parameters, in addition to the displacement thickness, δ^*, have been calculated at Michel's transition point and are subsequently employed as the initial values to propagate these boundary layer characteristics through the turbulent regime.

$$\frac{d\theta}{ds}+\frac{\theta}{V_e}\left(2+\frac{\delta^*}{\theta}\right)\frac{dV_e}{ds}=\frac{1}{2}c_f \tag{6}$$

$$c_f = 0.246\times 10^{-0.678H}\,\mathrm{Re}_\theta^{-0.268} \tag{7}$$

$$H(\lambda)=\begin{cases}2.61-3.75\lambda+5.24\lambda^2 & \text{for} \quad 0<\lambda<0.1\\ 2.088+\dfrac{0.0731}{\lambda+0.14} & \text{for} \quad -0.1<\lambda<0\end{cases} \tag{8}$$

$$\frac{1}{V_e}\frac{d}{dx}\left(V_e\theta H_1\right)=0.0306\left(H_1-3\right)^{-0.6169} \tag{9}$$

where

$$H_1=\begin{cases}3.3+0.8234\,(H-1.1)^{-1.287} & for \quad H>1.6\\ 3.3+1.5501\,(H-0.6778)^{-3.064} & for \quad H\leq 1.6\end{cases} \tag{10}$$

For an extensive review of the boundary layer theory, please refer to Blower and Wickenheiser [30].

In addition, during scenarios where a forward element's wake interacts with an element downstream, the boundary is assumed to continue from one element to the next. However, as a one-equation boundary layer theory is employed, the boundary layer growth cannot be modeled beyond separation. To overcome this issue, the rate of growth beyond the element's trailing edge is assumed to remain constant; subsequently, any element surfaces within the trailing edge plume are defined to resume the boundary layer in the current regime.

As the laminar, transition and turbulent regions have now been successfully modeled, the coefficient of friction, a dimensionless representation of the wall shear stress, τ_w, along the airfoil surface can be found from Eq. (9)

$$\tau_w = c_f\,\tfrac{1}{2}\rho V_e^2 \tag{X}$$

The tangential and normal forces are calculated using the pressure distribution and viscous forces applied to the airfoil surface. The coefficients of lift, drag, and moment can be subsequently calculated for each flap configuration through the integration of the pressure and wall shear stress incurred across airfoil's surfaces.

RESULTS

During the development of this aerodynamic model, the boundary layer models employed were validated through comparison to existing codes, JavaFoil, XFoil, and Pablo. However, due to the MFP containing multiple bodies, none of these other codes can model the boundary layer flow for these configurations, therefore the simulations were performed for the a single trailing edge profile with and without the integration of the iterative wake relaxation scheme. Each code simulated the airfoil geometries in the rest configuration, where $\alpha = 0°$ and $\delta = 0°$, for a Re = 3,000,000 to model the momentum thickness and coefficient of friction over the wing's surface. The APM and Pablo codes both implement Thwaites, Michel's and Head's as their flow regime boundary layer conditions, while JavaFoil implements the methodology developed by Eppler [50]. XFoil employs an interaction method, thereby coupling the resultant effects of the inviscid and viscous flows and the e^n transition method [51].

For each of the five methods compared, JavaFoil, XFoil, Pablo, and the APM with and without wake relaxation, the transition point can be identified by the rapid change in momentum thickness and coefficient of friction along the airfoil's surfaces, as seen in Fig. 6. The transition point for each panel code is defined by Michel's criterion along the upper and lower airfoil surfaces. The transition point of the APM with no wake relaxation scheme occurs downstream of the JavaFoil transition point at 18% and 9% for the upper and lower surfaces, respectively. In comparison, Pablo has a delayed transition point by 18% and 5%, respectively. The discrepancy in the transition point of Pablo and the APM is due to Pablo rounding the stagnation point to the nearest collocation point, therefore causing the velocity profile to be redistributed around the airfoil and causing the boundary layer to reach the transition condition after a shorter distance. XFoil showed transition 2.87% and 6.64% earlier than the APM without wake relaxation as the e^n method has been demonstrated to trigger the transition point earlier than other transition criteria [26]. In comparison between the APM with the integrated wake relaxation scheme, the upper and lower surface transition points occur 8% and 12%, respectively, further upstream. This is a result of the change of pressure distribution over the airfoil's surface due to the influence of the wake profile. The boundary layer method employed has demonstrated a reliable consistency with competitive codes, and was subsequently employed for the multi-element modeling.

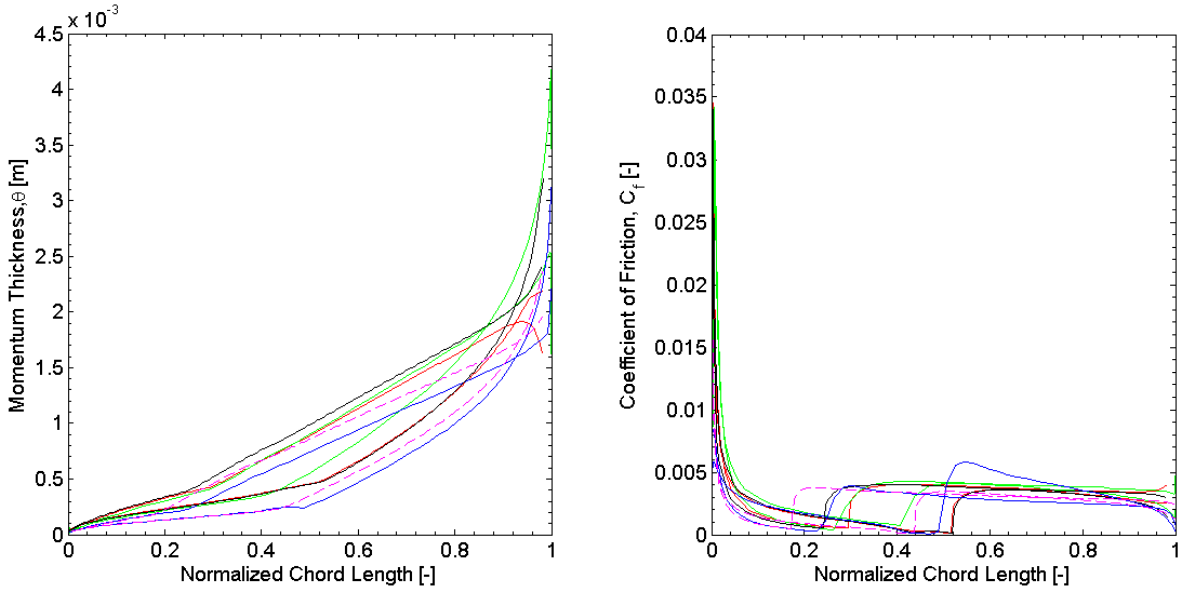

Figure 6: A comparasion between the growth of momentum thickness and coefficient of friction over a NACA 4412 geometry at an angle of attack, $\alpha = 0°$, trailing edge deflection $\delta = 0°$, at a Re = 3,000,000 for the APM with/without the iterative wake relaxation (red) and (magenta dashed) respectively, JavaFoil (green), Pablo (black), and XFoil (blue).

The flight coefficients are calculated for the STE airfoil between angles of attack ±16° in 2° increments, with the flap positioned in the rest position. Experimental data performed both at GW and previously by Abbott et al. [19]

are included in the assessment of the flight coefficients calculated by the APM. Abbott et al. reported data on the NACA 4412 airfoil at a Re=3e6, whereas the simulations performed by JavaFoil, Pablo and the APM were repeated at a Re=3.5e5 to accommodate for the flow characteristics that can be achieved in the GW wind tunnel. The APM with a wake relaxation scheme demonstrated consistency with the experimental data for all aerodynamic coefficients. Across the range of angles of attack, a maximum variation of ±4.5% for coefficient of lift was produced by the APM with the wake relaxation scheme, Fig. 7a. For the drag coefficient, a difference of 9% was calculated in comparison to the experimental data of Abbott et al., Fig. 7b. The coefficient of moment varies up to 22% in comparison to Abbott et al. across the angle of attack range -13° to 6°, Fig 7c. The APM with wake relaxation has been demonstrated to be a consistent improvement in comparison to the basic APM, when compared to experimental results.

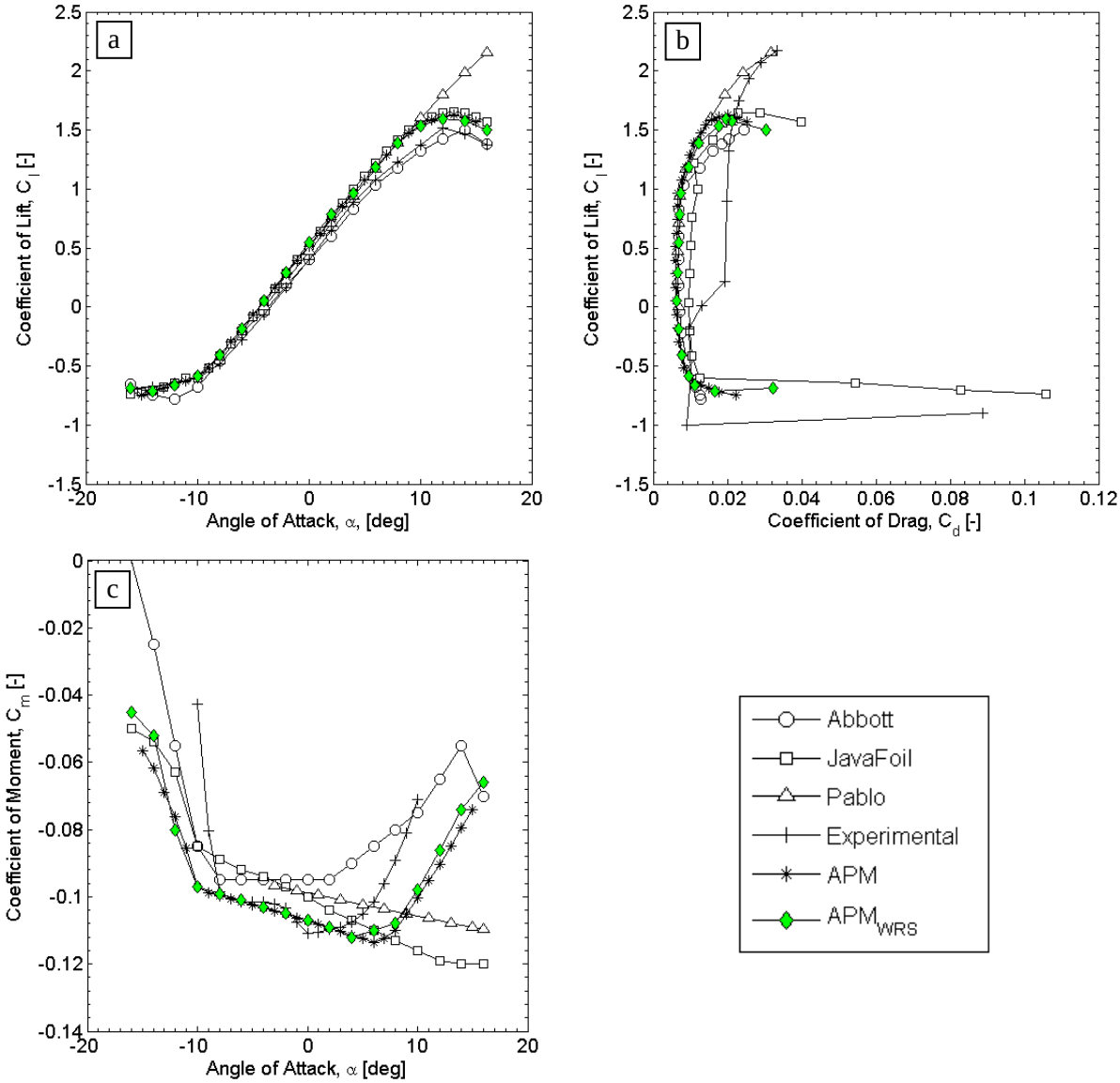

Figure 7: The coefficient of lift (a), drag (b) and moment (c) for a NACA4412 at Re = 350,000 for the APM with wake relaxation scheme (APM_{WRS}) against competitive codes and experimental studies [19]

CONCLUSIONS

This paper presents the development of an adaptive panel method with an iterative spatial relaxation scheme and integrated boundary layer for a two-dimensional multi-flap profile that can both mimic the geometries generated by a standard airfoil and generate complex profiles to manipulate the local flow. Due to the number of potential configurations available by the multi-flap profile, it is crucial to validate the basic geometries against airfoil configurations that have been extensively tested both computationally and experimentally. The implementation of the wake relaxation scheme has achieved an improved accuracy in the pressure distribution over the airfoil and enables flow separation and reattachment to be modeled between sequential elements.

The application of Thwaites, Michel's and Head's boundary layer theories enable the growth of the momentum thickness and coefficient of friction to be assessed while the airfoil is operating in the basic rest configuration, thereby mimicking a NACA 4412 geometry, or the complex multi-element geometries. The wake region modeling also accounts for the boundary layer growth over multiple surfaces through the identification of the reattachment regions, thereby improving the accuracy of the model. In addition, the regions of relaminarization due to adverse pressure gradients can also be assessed using the adaptive panel method, which becomes advantageous when airfoil profile is in a morphed configuration, where flow separation and reattachment can occur across the airfoil and wake geometry.

This methodology has been demonstrated to operate successfully in comparison to competitive codes while operating the basic configurations and closely tracks the trends given in experimental results. This aerodynamic solver can accurately accommodate for the multi-lifting surface designs that are present in bio-inspired aircraft design.

REFERENCES

[1] O. Bilgen, E. I. S. Flores, and M. I. Friswell, "Optimization of Surface-Actuated Piezocomposite Variable-Camber Morphing Wings," in *Smart Mater. Adapt. Struct. Intell. Syst.*, pp. 1–8 (2011) [doi:SMASIS2011-4971].

[2] G. E. Docketer and B. K. Hamilton, "Geometric Morphing Wing with Expandable Spars," 6622974, US Patent Office, Alexandria, VA, USA (2003).

[3] D. T. Grant, M. Abdulrahim, and R. Lind, "Flight Dynamics of a Morphing Aircraft Utilizing Independent Multiple-Joint Wing Sweep," *Int. J. Micro Air Veh.* **2**(2), 91–106 (2010) [doi:10.1260/1756-8293.2.2.91].

[4] J. E. Blondeau and D. J. Pines, "Pneumatic Morphing Aspect Ratio Wing," in *45th AIAA/ASME/ASCE/AHS/ASC Struct. Struct. Dyn. Mater. Conf.*, pp. 1–12, Palm Springs, CA (2004) [doi:10.2514/6.2004-1808].

[5] T. L. Hinshaw, "Analysis and Design of a Morphing Wing Tip using Multicellular Flexible Matrix Composite Adaptive Skins by," Virginia Polytechnic Institute and State University (2009).

[6] W. Williams and M. Harris, "The Challenges of Flight-Testing Unmanned Air Vehicles," in *Syst. Eng. Test Eval. Conf.*(October), Sydney, Australia (2002).

[7] W. Muller and G. Patone, "Air Transmissivity of Feathers," *J. Exp. Biol.* **201**, 2591–2599 (1998).

[8] D. W. Bechert, M. Bruse, W. Hage, and R. Meyer, "Fluid mechanics of biological surfaces and their technological application," *Naturwissenschaften* **87**(4), 157–171 (2000).

[9] T. J. Mueller, *Fixed and Flapping Wing Aerodynamics for Micro Air Vehicle Applications*, P. Zarchan, Ed., AIAA (2001).

[10] G. E. Hudson, P. J. Lanzillotti, and N. Dame, "Gross Anatomy of the Wing Muscles in the Family Corvidae," *Am. Midl. Nat.* **53**(1), 1–44 (1955).

[11] A. Alfred, *Sibley's Birding Basics*, Alfred A. Knopf, Inc. (2002).

[12] Necker, "Receptors in the Skin of the Wing of the Pigeon and Their Possible Role in Bird Flight," in *Biona Rep. 3 Bird Flight - Vogelflug*, W. Nachtigall, Ed., pp. 433–444, Gustav Fischer, Stuttgart, Germany (1985).

[13] W. Horster, "Histological and Electrophysiological Investigations on the Vibration-Sensitive Receptors (Herbst Corpuscles) in the Wing of the Pigeon (Columba livia)," *J. Comp. Physiol.* **166**, 663–673 (1990).

[14] T. Cebeci, "Calculation of Multielement Airfoils and Wings at High Lift," in *Advis. Gr. Aerosp. Res. Dev.*, AGARD, Banff, Canada (1993).

[15] A. M. Krumbein, "Automatic Transition Prediction and Application to High-Lift Multi-Element Configurations," *J. Aircr.* **42**(5), 1150–1164 (2005) [doi:10.2514/1.10329].

[16] W. Fritz, "Calculation of Maximum and High Lift Characteristics of Multi Element Airfoils," AGARD, Friedrichshafen, Germany (1993).
[17] S. E. Rogers, N. L. Wiltberger, and D. Kwak, "Efficient Simulation of Incompressible Viscous Flow over Multi-Element Airfoils" (1993).
[18] T. Cebeci, J. P. Shao, F. Kafyeke, and E. Laurendeau, *Computational Fluid Dynamics for Engineers*, 1st ed., Springer New York, New York, NY (2005).
[19] I. H. Abbott and A. E. von Doenhoff, *Theory of Wing Sections*, 1st ed., Dover Publications, New York (1959).
[20] J. Katz and A. Plotkin, *Low-Speed Aerodynamics*, 2nd ed., Cambridge University Press, New York (2001).
[21] R. Courant, *Dirichlet's Principle, Conformal Mapping, and Minimal Surfaces*, 1st ed., Dover Publications, New York, NY (2005).
[22] J. L. Hess, "Panel Methods in Computational Fluid Dynamics," *Annu. Rev. Fluid Mech.* **22**, 255–274 (1990) [doi:0066-4189/90/0115-0225].
[23] C. A. Cox, "Two Element Linear Strength Vortex Panel Method," pp. 1–17, California Polytechnic State University (2011).
[24] F. T. Johnson, "A General Panel Method for the Analysis and Design of Arbitrary Configurations in Incompressible Flows," Seattle, WA (1980) [doi:NAS2-7729].
[25] T. Cebeci, "An Interactive Boundary-Layer Approach to Multielement Airfoils at High Lift," *AIAA* (1992) [doi:AIAA 92-0404].
[26] R. Peltonen, "Viscous-Inviscid Method for Airfoil Analysis and Design for Aviation and Windmills," *J. Aircr.* **43**(4), 1069–1081 (2006).
[27] E. Besnard, B. Puech, D. Ivshin, O. Kural, and T. Cebeci, "Predictions of Stall and Post-Stall in Two- and Three-Dimensional Flows," *AIAA J.* (2000).
[28] C. J. Blower, W. Lee, and A. M. Wickenheiser, "The Development of a Closed-Loop Flight Controller with Panel Method Intgration for Gust Alleviation using Biomimetic Feathers on Aircraft Wings," in *SPIE*, pp. 1–13 (2012).
[29] C. J. Blower and A. M. Wickenheiser, "The Variations in Active Panel Location and Number for a Bioinspired Aircraft Gust Alleviation System," in *Smart Mater. Adapt. Struct. Intell. Syst.*, pp. 1–10 (2012) [doi:SMASIS2012-7994].
[30] C. J. Blower and A. M. Wickenheiser, "The Validation of a Generalized Aerodynamic Model for a Multi-Body Bio-Inspired Wing," in *Smart Mater. Adapt. Struct. Intell. Syst.*, pp. 1–11, ASME, Snowbird, UT (2013) [doi:SMASIS2013-3075].
[31] Y. Kim and K.-H. Kim, "Numerical Stability of Rankine Panel Method for Steady Ship Waves," *Ships Offshore Struct.* **2**(4), 299–306 (2007).
[32] Y. Kim, S. H. Kim, and T. Lucas, "Advanced Panel Method for Ship Wave Inviscid Flow Theory (SWIFT)," Bethesda, MD (1989).
[33] S. A. Yon, "Systematic Formulation and Analysis of 2-D Panel Methods," San Diego State University (1990).
[34] G. Bramesfeld, "A Higher Order Vortex-Lattice Method with a Force-Free Wake," Pennslyvania State University (2006).
[35] D. Basso, "Improvement of a Low-Order Panel Method by Far-Field COmputation of Iduced Drag for Arbitrary Non-Planar Wing Configurations," Universita Deglia Studi di Padovra (2013).
[36] J. G. Leishman, *Principles of Helicopter Aerodynamics*, 2nd ed., Cambridge Press, New York, NY (2006).
[37] M. Ribera and R. Celi, "Simulation Modeling of Unsteady Maneuvers using a Time Accurate Free Wake," in *VTOL Conf.*, American Helicopter Society (2004).
[38] D. L. Ashby, "Development and Validation of an Advanced Low-Order Panel Method" (1988).
[39] A. H. Ali, "Wake Roll-Up Behind Wings with Ground Effect," *Iraqi J. Mech. Mater. Eng.* **10**(2), 181–202 (2010).
[40] S. Gaggero and S. Brizzolara, "Exact Modeling of Trailing Vorticity in Panel Method for Marine Propeller," in *Int. Conf. Mar. Res. nd Transp.*(8), ICMRT, Ischia, Italy (2007).
[41] B. Maskew, "Program VSAERO Theory Document," Redmond, WA (1987).
[42] D. Coles and A. J. Wadcock, "Flying-Hot-Wire Study of Flow Past an NACA 4412 Airfoil at Maximum Lift," *AIAA J.* **17**(4), 321–329 (1979).
[43] R. M. Pinkerton, "The Variation with Reynolds Number of Pressure Distribution Over an Airfoil Section" (1938).

[44] J. Moran, *An Introduction to Theoretical and Computational Aerodynamics*, 1st ed., Dover Publications, New York (1984).
[45] F. M. White, *Viscous Fluid Flow*, 3rd ed., McGraw-Hill, New York (2006).
[46] R. Michel, "Etude de la Transition sur les Profiles d'Aile" (1951) [doi:1/1578A].
[47] P. M. Moretti and W. M. Kays, "Heat transfer to a turbulent boundary layer with varying free-stream velocity and varying surface temperature—an experimental study," *Int. J. Heat Mass Transf.* **8**(9), 1187–1202 (1965).
[48] K. Itoh, Y. Tsuji, H. Nakamura, and Y. Kukita, "Initial Free Surface Instabilities on a High-Speed Water Jet Simulating a Liquid-Metal Target," *Fusion Technol. A J. Am. Nucl. Soc. Eur. Nucl. Soc.* **36**(1), 69–84 (1999).
[49] K. Itoh, H. Nakamura, H. Kumamaru, and Y. Kukita, "Internal-Shear Mode Instabilities on High-Speed Liquid Jet , (II)," *Nucl. Sci. Technol.* **41**(8), 809–816 (2004).
[50] R. A. Eppler and D. M. Somers, "Supplement to: A computer program for the design and analysis of low-speed airfoils," NASA, Hampton, VA, pp. 1–36 (1980) [doi:NASA-TM-81862].
[51] M. Drela and H. Youngren, "XFoil Instruction Manual," MIT, Boston, MA (2001).